drones

Article

Adaptive Neural-Network-Based Nonsingular Fast Terminal Sliding Mode Control for a Quadrotor with Dynamic Uncertainty

Shurui Huang [1] and Yueneng Yang [1,2,*]

[1] College of Aerospace Science and Engineering, National University of Defense Technology, Changsha 410073, China
[2] College of Intelligence Science and Technology, National University of Defense Technology, Changsha 410073, China
* Correspondence: yangyueneng@163.com

Abstract: This paper proposes an adaptive neural-network-based nonsingular fast terminal sliding mode (NN-NFTSMC) approach to address the trajectory tracking control problem of a quadrotor in the presence of model uncertainties and external disturbances. First, the dynamic model of the quadrotor with uncertainty is derived. Then, a control scheme using nonsingular fast terminal sliding mode control (NFTSMC) is proposed to guarantee the finite-time convergence of the quadrotor to its desired trajectory. NFTSMC is firstly formulated for the case that the upper bound of the lumped uncertainty is known in advance. Under this framework, a disturbance observer by using the hyperbolic tangent nonlinear tracking differentiator (TANH-NTD) is designed to estimate the external interference, and a neural network (NN) approximator is used to develop an online estimate of the model uncertainty. Subsequently, adaptive algorithms are designed to compensate the approximation error and update the NN weight matrix. An NN-NFTSMC algorithm is formulated to provide the system with robustness to the model uncertainty and external disturbance. Moreover, Lyapunov-based approach is employed to prove the global stability of the closed-loop system and the finite-time convergence of the trajectory tracking errors. The results of a comparative simulation study with other recent methods illustrate the proposed control method reduces the chattering effectively and has remarkable performance.

Keywords: neural network; nonsingular fast terminal sliding mode; trajectory tracking; uncertainties and disturbances

Citation: Huang, S.; Yang, Y. Adaptive Neural-Network-Based Nonsingular Fast Terminal Sliding Mode Control for a Quadrotor with Dynamic Uncertainty. *Drones* **2022**, *6*, 206. https://doi.org/10.3390/drones6080206

Academic Editors: Yu Wu and Liguo Sun

Received: 5 July 2022
Accepted: 9 August 2022
Published: 12 August 2022

1. Introduction

Quadrotors have broad applications on military and civilian areas, such as environmental supervision, geological analysis, agricultural operations, search and rescue, and mail delivery [1,2]. In particular, they have promptly garnered special attention from the aviation research due to their advantageous characteristics such as lightweight structure, vertical take-off and landing, simple mechanical design, good maneuverability [3]. However, the trajectory tracking control of a quadrotor unmanned aerial vehicle (UAV) is a complicated problem. On the one hand, the quadrotor is an inherently nonlinear and multiple-input multiple-output (MIMO) system. On the other hand, the under-actuated properties lead to strong coupling among state variables. Furthermore, quadrotor dynamics involve parameter uncertainties and external disturbances, leading to potentially unstable flight trajectories [4].

There are several control methods for the trajectory tracking problem of quadrotors that have been explored in previous research. Linear control methods, such as proportional-derivative (PD), proportional integral derivative (PID) and linear quadratic (LQR) are presented in Refs [5–7]. However, these linear control techniques cannot ensure the stability of the system when the vehicle moves away from the operating domain. In addition, these control approaches have limited capabilities of coupling alleviation and interference suppression.

To obtain an accurate flight path trajectory when the quadrotor maneuvers rapidly, a variety of nonlinear flight control methods have been developed, which can overcome the drawbacks of the linear control approaches, such as backstepping control [8], feedback linearization [9], sliding mode control (SMC) [10]. Of these methods, SMC has been proved to be an attractive method for trajectory tracking control, which can compensate for the model uncertainties and external disturbances. In other words, the main benefit of the SMC technique is low sensitivity to parameter variations and dynamic uncertainties. Based on the quadrotor model subjected to parametric uncertainties and external disturbances, the fuzzy logic system (FLS) was employed in the structure of SMC to schedule the switching gain and suppress the chattering [11]. The SMC method with the optimized radial basis function neural networks (RBFNN) approximator was proposed for a 6-DOF quadrotor [12]. In addition, the SMC technique also has been applied in other fields, such as attitude tracking control of spacecraft [13], trajectory tracking for robotic airships [14] and autonomous underwater vehicles [15].

For many practical systems like the quadrotor, it is required that the designed control system must fulfill some performance index, such as convergence speed and steady-state error [16]. Whereas, the ordinary sliding mode control can only drive the system state converge progressively, it cannot quickly reach the origin within a finite-time. To obtain the finite-time convergence, terminal sliding mode control (TSMC) has been developed, which adopt nonlinear sliding surfaces. Based on a quadrotor system in the presence of external disturbance, a robust fuzzy TSMC method is developed to track the predefined flight path [17]. To further improve the convergence speed, a fast terminal sliding mode (FTSMC) has been proposed. In Ref. [18], a robust control method which consisted of the FTSMC method and super twisting reaching law, is proposed for the quadrotor position and attitude tracking. However, the traditional FTSMC method suffers from the singularity problem due to the terms with negative fraction power. To handle the singularity problem, a nonsingular fast terminal sliding mode control (NFTSMC) method is recently developed. Based on the orbit-coupling spacecraft model, an improved NFTSMC method combined with a continuous differentiable constraint function was designed to solve the problem of the spacecraft final approach [19]. Further, an adaptive NFTSMC method for controlling the position and attitude of the smart flexible satellite [20]. Combined with the fully tuned RBFNN, a finite-time control scheme using NFTSMC algorithm is proposed for redundant parallel manipulators [21].

Motivated by the aforementioned analysis and inspired by Refs. [22,23], this paper presents an adaptive neural-network-based nonsingular fast terminal sliding mode control (NN-NFTSMC) scheme, to address the problem of trajectory tracking for a quadrotor in the presence of inertial uncertainties and external disturbances. First, this paper presents a quadrotor dynamic model with parametric uncertainty and unknown disturbances. For the inertial uncertainties and external disturbances, the NFTSMC method can guarantee convergence of the tracking errors in finite-time. However, the quadrotor dynamic model is usually uncertain and the bounds of the uncertainties and disturbances are often unknown. Therefore, under the framework of NFTSMC, a nonlinear disturbance observer is designed by using a hyperbolic tangent nonlinear tracking differentiator (TANH-NTD) to estimate the external disturbance. The neural network (NN) technique is utilized to estimate the model uncertainties due to its strong nonlinear fitting ability. Furthermore, adaptive algorithms are applied to automatically adjust the parameters of the controller to estimate the unknown upper bound of the approximation error. Also, by employing the designed controller, the chattering generated obviously in the conventional SMC is alleviated, without losing the tracking precision and robustness property.

The main contributions and the key features of this paper are summarized as follows:

(1) A NFTSMC method is adopted to guarantee that the quadrotor system acquires high-speed response, accurate tracking and strong robustness. Furthermore, the NFTSMC method can overcome the singularity problem that exists in the normal FTSMC approach.

(2) A TANH-NTD disturbance observer and an NN approximator are formulated to provide an online estimate of the external disturbance and model uncertainties, which can allows for the relaxation of the requirement of prior knowledge about the bound of the uncertainties and disturbances, thus reducing the difficulty in modeling the system in practice.

(3) The NN-NFTSMC control method acquire high-speed response, accurate tracking and strong robustness, but also alleviate the negative effect of chattering.

The remainder of the paper is organized as follows. Section 2 describes the preliminaries and problem formulation. Section 3 presents the formulation of the controller NN-NFTSMC to be used in the trajectory tracking of the quadrotor. Section 4 presents the results of simulations to illustrate the effectiveness of the designed control method. Finally, Section 5 concludes the paper.

2. Preliminaries and Problem Formulation

2.1. Preliminaries

The following notations are adopted throughout this paper. $|\cdot|$ represent the absolute value of each element of a vector. $\|\cdot\|$ denotes the Euclidean norm of a vector. $\lambda_{\max}(\cdot)$ denotes the maximum element of a vector or the maximum eigenvalue of a matrix; $\lambda_{\min}(\cdot)$ denotes the minimum element of a vector or the minimum eigenvalue of a matrix. For a variable vector $\boldsymbol{q} = [q_1, \cdots, q_n]^T \in \mathcal{R}^n$, the function $\text{sign}^{\alpha}(\boldsymbol{q})$ is denoted as

$$\text{sign}^{\alpha}(\boldsymbol{q}) = |\boldsymbol{q}|^{\alpha}\text{sign}(\boldsymbol{q}) = [|q_1|^{\alpha}\text{sign}(q_1), \cdots, |q_n|^{\alpha}\text{sign}(q_n)]^T \tag{1}$$

Then, it is easy to obtain

$$\frac{\mathrm{d}(\text{sign}^{\alpha}(\boldsymbol{q}))}{\mathrm{d}t} = \alpha|\boldsymbol{q}|^{\alpha-1}\dot{\boldsymbol{q}} \tag{2}$$

2.2. Kinematics and Dynamics

The structure of the studied quadrotor model is shown in Figure 1, which consists of a rigid cross-frame and four propellers. The kinematics model that describes the position and attitude of the quadrotor is given by [4]:

$$\begin{cases} \dot{\boldsymbol{\xi}} = \boldsymbol{R}_t \boldsymbol{v}_{\boldsymbol{a}} \\ \dot{\boldsymbol{\eta}} = \boldsymbol{R}_r \boldsymbol{\omega}_{\boldsymbol{b}} \end{cases} \tag{3}$$

where $\boldsymbol{\xi} = [x, y, z]^T$ and $\boldsymbol{\eta} = [\phi, \theta, \psi]^T$ denote the quadrotor position and attitude in the inertial frame ($O_e - x_e y_e z_e$), $\boldsymbol{v_a} = [u, v, w]^T$ and $\boldsymbol{\omega_b} = [p, q, r]^T$ represent the speed and angular velocity with respect to the body frame ($O_b - x_b y_b z_b$), $\boldsymbol{R}_t$ and $\boldsymbol{R}_r$ is the direction cosine matrix and transformation matrix respectively, whose expressions can be found in Ref. [24].

The rigid quadrotor system modeling described by Euler dynamic equations can be expressed as follows [25].

$$\begin{cases} \boldsymbol{J}\ddot{\boldsymbol{\eta}} = -\boldsymbol{\eta}^T \times \boldsymbol{J}\boldsymbol{\eta} + \boldsymbol{\tau} - \boldsymbol{\tau}_c - \boldsymbol{\tau}_a + \boldsymbol{d}_{\boldsymbol{\eta}} \\ m\ddot{\boldsymbol{\xi}} = \boldsymbol{R}_t u - mg\boldsymbol{e}_z - \boldsymbol{f}_D + \boldsymbol{d}_{\boldsymbol{\xi}} \end{cases} \tag{4}$$

where $\boldsymbol{e_z} = [0, 0, 1]^T$. m is the total mass, $\boldsymbol{J}$ is the symmetric inertia matrix, u denotes the gross thrust generated by four rotors with respect to the body frame, g denotes the vector of gravity acceleration, $\boldsymbol{\tau}$ denotes the rotation torque produced by four propellers, $\boldsymbol{\tau}_c$ denotes the resultant moment generated by the gyroscopic effects. $\boldsymbol{\tau}_a$ denotes the resultant of aerodynamic friction torque, $\boldsymbol{f}_D$ denotes the aerodynamic force, $\boldsymbol{d}_{\boldsymbol{\eta}}$ and $\boldsymbol{d}_{\boldsymbol{\xi}}$ are the unknown external disturbances.

In this study, the additional parameter uncertainties of the quadrotor system can be expressed as follows:

$$J = J_0 + \Delta J,\ m = m_0 + \Delta m \tag{5}$$

where J_0 and m_0 denote the known inertial matrix and mass; ΔJ and Δm represent the bounded uncertainties.

Then, the dynamic system described by Equation (4) can be rewritten as:

$$\begin{cases} J_0\ddot{\eta} = -\dot{\eta}^T \times J_0\dot{\eta} + \tau - \tau_c - \tau_a + d_\eta - \Delta J\ddot{\eta} - \dot{\eta}^T \times \Delta J\dot{\eta} \\ m_0\ddot{\xi} = R_t u - m_0 g e_z - f_D + d_\xi - \Delta m g e_z - \Delta m\ddot{\xi} \end{cases} \tag{6}$$

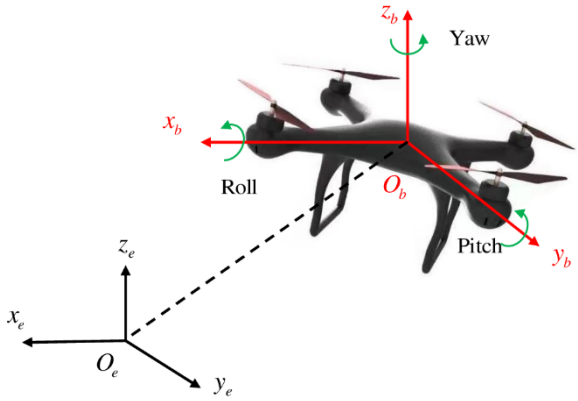

Figure 1. Structure of the quadrotor.

2.3. Problem Formulation

The quadrotor is an under-actuated system, which has six outputs and four control inputs. In order to facilitate the controller design, a virtual control input $v = [v_x, v_y, v_z]^T$ is introduced as:

$$\begin{bmatrix} v_x \\ v_y \\ v_z \end{bmatrix} = \begin{bmatrix} (\cos\phi \sin\theta \cos\psi + \sin\phi \sin\psi)\frac{u}{m} \\ (\cos\phi \sin\theta \sin\psi - \sin\phi \cos\psi)\frac{u}{m} \\ \cos\phi \cos\theta \frac{u}{m} - g \end{bmatrix} \tag{7}$$

For simplicity, the quadrotor system can be deformed as follows:

$$\ddot{x} = F + Gu + D + d \tag{8}$$

with

$$F = \begin{bmatrix} \frac{-\dot{\eta}^T \times J_0\dot{\eta} - \tau_c - \tau_a}{J_0} \\ \frac{-mge_z - f_D}{m_0} \end{bmatrix}, G = \begin{bmatrix} \frac{1}{J_0} & 0_{3\times3} \\ 0_{3\times3} & \frac{R_t}{m_0} \end{bmatrix}, D = \begin{bmatrix} \frac{-\Delta J\ddot{\eta} - \dot{\eta}^T \times \Delta J\dot{\eta}}{J_0} \\ \frac{-\Delta m g e_z - \Delta m\ddot{\xi}}{m_0} \end{bmatrix}, d = \begin{bmatrix} d_\eta \\ d_\xi \end{bmatrix} \tag{9}$$

where, $x = [\eta^T, \xi^T]^T$ is the state vector; $u = [\tau_\phi, \tau_\theta, \tau_\psi, v_x, v_y, v_z]^T$ is the input vector; D is the model uncertainty term; d denotes the external disturbance vector.

Then, by setting the desired pitch angle ψ_d, the desired roll angle ϕ_d, desired pitch θ_d angle can be obtained [25]:

$$\phi_d = \sin^{-1}\left(\frac{v_x \sin(\psi_d) - v_y \cos(\psi_d)}{v_z + g}\right),\ \theta_d = \tan^{-1}\left(\frac{v_x \cos(\psi_d) + v_y \sin(\psi_d)}{v_z + g}\right) \tag{10}$$

By setting the desired state $x_d = [\phi_d, \theta_d, \psi_d, x_d, y_d, z_d]^T$, the tracking errors are defined as:

$$E_1 = x - x_d,\ E_2 = \dot{x} - \dot{x}_d \tag{11}$$

The control purpose of this work is formulated as follows: given the initial system state x_0, and the desired state x_d, design a robust controller to stabilize the vehicle subjected

to the model uncertainties and external disturbances. The vectors of tracking errors given by Equation (11), are required to converge to zero in a finite-time, i.e.,:

$$\lim_{t\to t_f}\|\boldsymbol{E}_1\| = 0, \lim_{t\to t_f}\|\boldsymbol{E}_2\| = 0 \tag{12}$$

3. NN-NFTSMC Controller Design

This section is devoted to the controller system design of the quadrotor. NFTSMC technique is adopted to design the trajectory tracking controller. Under this control framework, the hyperbolic tangent nonlinear tracking differentiator (TANH-NTD) and RBFNN are developed to respectively approximate external disturbances and system uncertainties. Adapting algorithms are introduced to update the weight matrix of RBFNN and estimate the upper bound of the approximation errors.

3.1. NFTSMC Design

The trajectory tracking errors are defined as:

$$\boldsymbol{e} = \boldsymbol{x} - \boldsymbol{x}_d \tag{13}$$

The first derivative of the trajectory tracking errors is given by:

$$\dot{\boldsymbol{e}} = \dot{\boldsymbol{x}} - \dot{\boldsymbol{x}}_d \tag{14}$$

A nonsingular fast terminal sliding surface is chosen as follows:

$$\boldsymbol{s} = \boldsymbol{e} + \boldsymbol{\alpha}\text{sign}^{\gamma_1}(\boldsymbol{e}) + \boldsymbol{\beta}\text{sign}^{\gamma_2}(\dot{\boldsymbol{e}}) \tag{15}$$

where $\boldsymbol{\alpha} = \text{diag}(\alpha_1, \alpha_2, \alpha_3, \alpha_4, \alpha_5, \alpha_6)$ and $\boldsymbol{\beta} = \text{diag}(\beta_1, \beta_2, \beta_3, \beta_4, \beta_5, \beta_6)$ are positive definite matrices, γ_1 and γ_2 are positive odd constants, satisfying $1 < \gamma_1 < 2$ and $\gamma_1 > \gamma_2$.

Remark 1. *In the above-mentioned sliding manifold design, when the system states are far from the equilibrium states, $\boldsymbol{\alpha}\text{sign}^{\gamma_1}(\boldsymbol{e})$ has a dominant position and ensures a high convergence rate, compared with $\boldsymbol{\beta}\text{sign}^{\gamma_2}(\dot{\boldsymbol{e}})$; when the system states approach the equilibrium states, $\boldsymbol{\beta}\text{sign}^{\gamma_2}(\dot{\boldsymbol{e}})$ guarantees the finite-time convergence.*

The time derivative of the sliding surface can be calculated as:

$$\dot{\boldsymbol{s}} = \dot{\boldsymbol{e}} + \boldsymbol{\alpha}\gamma_1|\boldsymbol{e}|^{\gamma_1-1}\dot{\boldsymbol{e}} + \boldsymbol{\beta}\gamma_2|\dot{\boldsymbol{e}}|^{\gamma_2-1}(\boldsymbol{F}+\boldsymbol{G}\boldsymbol{u}+\boldsymbol{D}+\boldsymbol{d}-\ddot{\boldsymbol{x}}_d) \tag{16}$$

Assumption 1. *The total dynamic uncertainties are assumed to be bounded, satisfying the following inequalities:*

$$\|\boldsymbol{D}\| + \|\boldsymbol{d}\| \le \rho \tag{17}$$

where ρ is a finite positive constant.

Based on the sliding surface given by Equation (15), the equivalent control law is designed as follows

$$\boldsymbol{u}_{eq} = -\boldsymbol{G}^{-1}\left(\boldsymbol{F} + \ddot{\boldsymbol{x}}_d - \frac{1}{\boldsymbol{\beta}\gamma_2}|\dot{\boldsymbol{e}}|^{2-\gamma_2}\left(1 + \boldsymbol{\alpha}\gamma_1|\boldsymbol{e}|^{\gamma_1-1}\right)\text{sign}(\dot{\boldsymbol{e}})\right) \tag{18}$$

Based on Assumption 1, the switching control law is given by:

$$\boldsymbol{u}_s = -\boldsymbol{K}_1\boldsymbol{s} - \boldsymbol{K}_2\text{sign}(\boldsymbol{s}) \tag{19}$$

where $\boldsymbol{K}_1 = \mathrm{diag}(K_{11}, K_{12}, K_{13}, K_{14}, K_{15}, K_{16})$ is a positive definite matrix $K_{1i} > 0$ (i = 1,2,3,4,5,6) is the design parameter, $\boldsymbol{K}_2 = \mathrm{diag}(K_{21}, K_{22}, K_{23}, K_{24}, K_{25}, K_{26})$ is the switching gain matrix, and $K_{2i} > 0$ (i = 1,2,3,4,5,6) is a positive constant, which satisfies:

$$K_{2i} = \lambda_{\max}(\boldsymbol{D}) + \lambda_{\max}(\boldsymbol{d}) + \delta \tag{20}$$

where δ is a small positive constant.

Hence, the NFTSMC control law for the quadrotor system is designed as:

$$\boldsymbol{u} = -\boldsymbol{G}^{-1}\left(\boldsymbol{F} - \ddot{\boldsymbol{x}}_d + \frac{1}{\gamma_2}|\dot{\boldsymbol{e}}|^{2-\gamma_2}\boldsymbol{\beta}^{-1}\left(1 + \boldsymbol{\alpha}\gamma_1|\boldsymbol{e}|^{\gamma_1-1}\right)\mathrm{sign}(\dot{\boldsymbol{e}}) + \boldsymbol{K}_1\boldsymbol{s} + \boldsymbol{K}_2\mathrm{sign}(\boldsymbol{s})\right) \tag{21}$$

The control scheme of the NFTSMC technique for trajectory tracking is indicated in Figure 2.

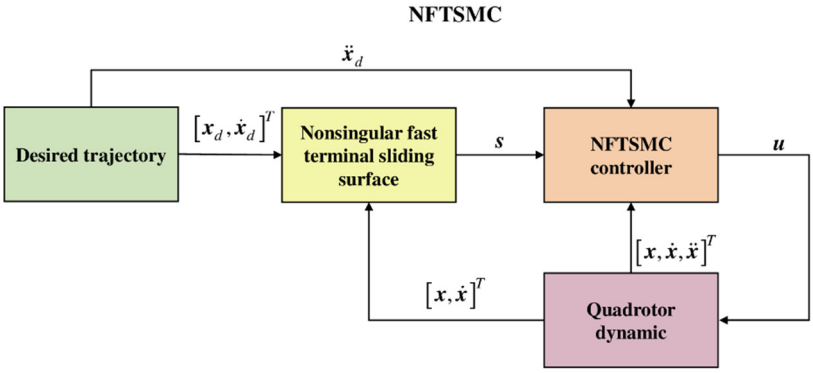

Figure 2. Block diagram of NFTSMC.

Lemma 1. [26] *Suppose there exists a positive definite Lyapunov function $V(\chi)$, which fulfills the inequation $\dot{V}(\chi) + k_1 V(\chi) + k_2 V^{k_3}(\chi) \leq 0$ where $k_1, k_2 > 0$ and $0 < k_3 < 1$. Let $V_0(\chi)$ be the initial value of $V(\chi)$, then the system state $\chi(t)$ converges to zero in finite time. The settling time T satisfies:*

$$T \leq \frac{1}{k_1(1-k_3)} \ln \frac{k_1 V_0^{1-k_3}(\chi) + k_2}{k_2} \tag{22}$$

Theorem 1. *Considering the nonlinear dynamic system given by Equation (8) and the sliding surface chosen as Equation (15), if the NFTSMC controller is designed as Equation (21), then the closed-loop system is stable and the tracking error can converge to zero in finite time.*

Proof. The candidate Lyapunov function is considered as:

$$V_1 = \frac{1}{2}\boldsymbol{s}^T\boldsymbol{s} \tag{23}$$

Differentiating Equation (23) with respect to time yields:

$$\dot{V}_1 = \boldsymbol{s}^T\dot{\boldsymbol{s}} \tag{24}$$

Substituting Equations (16) and (21), the above equation is converted to:

$$\begin{aligned} \dot{V}_1 &= \boldsymbol{s}^T\left(\dot{\boldsymbol{e}} + \boldsymbol{\alpha}\gamma_1|\boldsymbol{e}|^{\gamma_1-1}\dot{\boldsymbol{e}} + \boldsymbol{\beta}\gamma_2|\dot{\boldsymbol{e}}|^{\gamma_2-1}(\boldsymbol{F}+\boldsymbol{G}\boldsymbol{u}+\boldsymbol{D}+\boldsymbol{d}-\ddot{\boldsymbol{x}}_d)\right) \\ &= -\boldsymbol{\beta}\gamma_2|\dot{\boldsymbol{e}}|^{\gamma_2-1}\boldsymbol{K}_1\boldsymbol{s}^T\boldsymbol{s} + \boldsymbol{\beta}\gamma_2|\dot{\boldsymbol{e}}|^{\gamma_2-1}\left(\boldsymbol{s}^T(\boldsymbol{D}+\boldsymbol{d}) - \boldsymbol{s}^T\boldsymbol{K}_2\mathrm{sign}(\boldsymbol{s})\right) \end{aligned} \tag{25}$$

After simple calculation, the following can be obtained:

$$\begin{aligned}\dot{V}_1 &\leq -\gamma_2\boldsymbol{\beta}\left|\dot{\boldsymbol{e}}\right|^{\gamma_2-1}\boldsymbol{K}_1\boldsymbol{s}^T\boldsymbol{s} - \gamma_2\delta\boldsymbol{\beta}\left|\dot{\boldsymbol{e}}\right|^{\gamma_2-1}\|\boldsymbol{s}\| \\ &\leq -2\gamma_2\lambda_{\min}(\boldsymbol{K}_1)\lambda_{\min}(\boldsymbol{\beta})\lambda_{\min}(\left|\dot{\boldsymbol{e}}\right|^{\gamma_2-1})V_1 - \sqrt{2}\gamma_2\delta\lambda_{\min}(\boldsymbol{\beta})\lambda_{\min}(\left|\dot{\boldsymbol{e}}\right|^{\gamma_2-1})V_1^{1/2}\end{aligned} \tag{26}$$

By defining $\mu_1 = 2\gamma_2\lambda_{\min}(\boldsymbol{K}_1)\lambda_{\min}(\boldsymbol{\beta})\lambda_{\min}(\left|\dot{\boldsymbol{e}}\right|^{\gamma_2-1})$ and $\mu_2 = \sqrt{2}\gamma_2\delta\lambda_{\min}(\boldsymbol{\beta})\lambda_{\min}(\left|\dot{\boldsymbol{e}}\right|^{\gamma_2-1})$, the following inequation is obtained:

$$\dot{V}_1 \leq \mu_1 V_1 - \mu_2 V_1^{1/2} \tag{27}$$

Consequently, according to Lemma 1 and Lyapunov stability theory, it can be said that the NFTSM sliding manifold $\boldsymbol{s}(t)$ can converge to zero in finite time. This completes the proof. □

3.2. NN-NFTSMC Design

The proposed NFTSMC has provided an effective control method for the quadrotor system. In the design of NFTSMC, it is assumed that the upper bound of the lumped uncertainties is known in advance. In practical applications, the precise upper bound information is usually difficult to obtain. In order to compensate for the uncertainties existing in the actual system, the disturbance observer and the RBFNN approximator are designed to estimate the external disturbances $\boldsymbol{d}$ and the model uncertainties $\boldsymbol{D}$ respectively. Under the structure of NFTSMC, the NN-NFTSMC is designed with the disturbance observer and the RBFNN approximator.

A nonlinear disturbance observer using the TANH-NTD is designed as follow [27]:

$$\begin{cases} \ddot{\hat{\boldsymbol{x}}} = \boldsymbol{F} + \boldsymbol{G}\boldsymbol{u} + \boldsymbol{D} + \hat{\boldsymbol{d}} \\ \dot{\hat{\boldsymbol{d}}} = -\boldsymbol{R}^T\boldsymbol{R}\left(\boldsymbol{a}_1\tanh\left(\boldsymbol{b}_1\left(\dot{\hat{\boldsymbol{x}}} - \dot{\boldsymbol{x}}\right)\right) + \boldsymbol{a}_2\tanh\left(\boldsymbol{R}^{-1}\boldsymbol{b}_2\hat{\boldsymbol{d}}\right)\right) \end{cases} \tag{28}$$

where $\boldsymbol{R}$, $\boldsymbol{a}_1$, $\boldsymbol{a}_2$, $\boldsymbol{b}_1$ and $\boldsymbol{b}_2$ are positive definite diagonal matrices, $\dot{\hat{\boldsymbol{x}}}$ and $\hat{\boldsymbol{d}}$ are respectively estimates of $\dot{\boldsymbol{x}}$ and $\boldsymbol{d}$.

The approach of self-stable region is provided to prove the convergence of the disturbance observer designed as Equation (28) in Ref. [28].

Remark 2. *The existence of the unknown disturbances makes the stabilization of the quadrotor more difficult. In this study, a disturbance observer based on TANH-NTD is proposed to compensate the external disturbance in real time. By selecting the proper values of* $\boldsymbol{R}$, $\boldsymbol{a}_1$, $\boldsymbol{a}_2$, $\boldsymbol{b}_1$ *and* $\boldsymbol{b}_2$, *the disturbance observer can estimate the corresponding disturbance* $\boldsymbol{d}$. *Then, the approximation error* $\boldsymbol{\varepsilon}_n$ *of the disturbance observer is defined as* $\boldsymbol{\varepsilon}_n = \boldsymbol{d} - \hat{\boldsymbol{d}}$.

RBFNN is a well-known approach for the approximation of a nonlinear function. An RBFNN is a three-layer feedforward neural networks, which includes an input layer, a hidden layer with a nonlinear activation function and an output layer. The activation function $\boldsymbol{h}$, which is selected as Gaussian function, is expressed as:

$$h_j(\boldsymbol{r}) = \exp\left(\frac{\|\boldsymbol{r} - \boldsymbol{c}_j\|^2}{\sigma_j^2}\right), j = 1, 2, \cdots, m \tag{29}$$

where $\boldsymbol{r}$ is the input of the RBFNN, $\boldsymbol{c}_j$ is the center of the neuron, and σ_j is the width of Gaussian function for neural net j.

Lemma 2. [29] *For any positive constant* ε, *there always exists a RBFNN, which guarantees the approximation error ultimately converges to an adequate small compact.*

$$\sup_{\chi\in o}|f(\chi) - y(\chi)| < \varepsilon \tag{30}$$

where $f(\chi)$ is a continuous function which is defined on a compact set o, and $y(\chi)$ is the output of the RBFNN.

According to Lemma 2, the RBFNN is adopted to compensate for the model uncertainties $\boldsymbol{D}$, which can be expressed as follow:

$$\boldsymbol{D} = \boldsymbol{W}^T \boldsymbol{h} + \boldsymbol{\varepsilon}_m \tag{31}$$

where $\boldsymbol{W}$ is the optimal weight matrix, and $\boldsymbol{\varepsilon}_m$ denotes the approximation error.

The input vector of the RBFNN is chosen as:

$$\boldsymbol{r} = [\boldsymbol{x}, \dot{\boldsymbol{x}}, \ddot{\boldsymbol{x}}] \tag{32}$$

Then, the output vector of the RBFNN is

$$\hat{\boldsymbol{D}} = \hat{\boldsymbol{W}}^T \boldsymbol{h} \tag{33}$$

where $\hat{\boldsymbol{W}}$ is the estimation of the best weight matrix $\boldsymbol{W}$.

Assumption 2. *It is assumed that there exists a positive constant η, which satisfies the following inequation:*

$$\|\boldsymbol{\varepsilon}_m\| + \|\boldsymbol{\varepsilon}_n\| \leq \eta \tag{34}$$

where $\boldsymbol{\varepsilon}_m$ and $\boldsymbol{\varepsilon}_n$ denote the approximation errors of RBFNN and the disturbance observer respectively.

Based on the Equations (33) and (28), the control law in Equation (21) is rewritten as follows:

$$\boldsymbol{u} = -\boldsymbol{G}^{-1}\left(\boldsymbol{F} + \hat{\boldsymbol{D}} + \hat{\boldsymbol{d}} - \ddot{\boldsymbol{x}}_d + \frac{1}{\boldsymbol{\beta}\gamma_2}|\dot{\boldsymbol{e}}|^{2-\gamma_2}\left(1 + \boldsymbol{\alpha}\gamma_1|\boldsymbol{e}|^{\gamma_1 - 1}\right)\text{sign}(\dot{\boldsymbol{e}}) + \boldsymbol{K}_1\boldsymbol{s} + \boldsymbol{K}_2\text{sign}(\boldsymbol{s})\right) \tag{35}$$

With the adapting laws:

$$\dot{\hat{\boldsymbol{W}}} = \gamma_2 \boldsymbol{\Gamma}\boldsymbol{\beta}|\dot{\boldsymbol{e}}|\boldsymbol{h}\boldsymbol{s}^T \,,\ \dot{\hat{\eta}} = \lambda\boldsymbol{\beta}|\boldsymbol{s}|^T|\dot{\boldsymbol{e}}|^{\gamma_2 - 1} \tag{36}$$

where $\boldsymbol{\Gamma}$ is a positive definite matrix, and λ is a positive constant.

The block diagram of the NN-NFTSMC technique for trajectory tracking is illustrated in Figure 3.

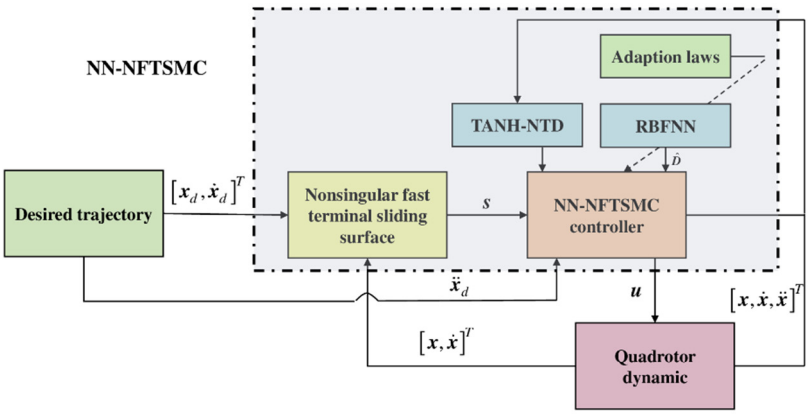

Figure 3. Block diagram of NN-NFTSMC.

Theorem 2. *For the quadrotor system subjected to the disturbances and model uncertainties described by Equation (8), if the nonsingular terminal sliding surface is selected as Equation (15) and the NN-NFTSMC controller is designed as Equation (35), in which the total dynamic uncertainties are estimated by Equations (28) and (33), and the adaption laws are selected as Equation (36), then*

the stability of the closed-loop system is guaranteed and the tracking errors converge to zero in finite time.

Proof. Select following Lyapunov function candidate V_2

$$V_2 = \frac{1}{2}\boldsymbol{s}^T\boldsymbol{s} + \frac{1}{2}\mathrm{tr}(\widetilde{\boldsymbol{W}}^T\boldsymbol{\Gamma}^{-1}\widetilde{\boldsymbol{W}}) + \gamma_2\frac{1}{2\lambda}\widetilde{\eta}^2 \tag{37}$$

where $\widetilde{\boldsymbol{W}} = \boldsymbol{W} - \hat{\boldsymbol{W}}$ and $\widetilde{\eta} = \eta - \hat{\eta}$. Through the previous analysis, it is clear that $\dot{\widetilde{\boldsymbol{W}}} = -\dot{\hat{\boldsymbol{W}}}$ and $\dot{\widetilde{\eta}} = -\dot{\hat{\eta}}$.

Differentiating Equation (37) yields:

$$\dot{V}_2 = \boldsymbol{s}^T\dot{\boldsymbol{s}} + \mathrm{tr}(\widetilde{\boldsymbol{W}}^T\boldsymbol{\Gamma}^{-1}\dot{\widetilde{\boldsymbol{W}}}) + \gamma_2\frac{1}{\lambda}\widetilde{\eta}\dot{\widetilde{\eta}} \tag{38}$$

By substituting Equation (16) into the Equation (38), the following equation can be obtained:

$$\dot{V}_2 = \boldsymbol{s}^T\Big(\dot{\boldsymbol{e}} + \boldsymbol{\alpha}\gamma_1|\boldsymbol{e}|^{\gamma_1-1}\dot{\boldsymbol{e}} + \boldsymbol{\beta}\gamma_2|\dot{\boldsymbol{e}}|^{\gamma_2-1}\ddot{\boldsymbol{e}}\Big) + \mathrm{tr}(\widetilde{\boldsymbol{W}}^T\boldsymbol{\Gamma}^{-1}\dot{\widetilde{\boldsymbol{W}}}) + \gamma_2\frac{1}{\lambda}\widetilde{\eta}\dot{\widetilde{\eta}} \tag{39}$$

By placing the NN-NFTSMC control law in Equation (35) and the adaptive laws in Equation (36) into the above equation, the following equation is obtained.

$$\begin{aligned}\dot{V}_2 &= \gamma_2\boldsymbol{\beta}|\dot{\boldsymbol{e}}|^{\gamma_2-1}\boldsymbol{s}^T((\boldsymbol{\varepsilon}_m + \boldsymbol{\varepsilon}_n) - \boldsymbol{K}_1\boldsymbol{s} - \hat{\eta}\mathrm{sign}(\boldsymbol{s})) \\ &+\mathrm{tr}\widetilde{\boldsymbol{W}}^T\Big(\gamma_2\boldsymbol{\beta}^T|\dot{\boldsymbol{e}}|^{\gamma_2-1}\boldsymbol{h}\boldsymbol{s}^T + \boldsymbol{\Gamma}^{-1}\Big(-\boldsymbol{\Gamma}\gamma_2\boldsymbol{\beta}^T|\dot{\boldsymbol{e}}|^{\gamma_2-1}\boldsymbol{h}\boldsymbol{s}^T\Big)\Big) + \gamma_2\tfrac{1}{\lambda}\widetilde{\eta}\boldsymbol{\beta}|\boldsymbol{s}|^T|\dot{\boldsymbol{e}}|^{\gamma_2-1}\end{aligned} \tag{40}$$

Simplifying Equation (40) leads to the following relation.

$$\dot{V}_2 = \gamma_2\boldsymbol{\beta}|\dot{\boldsymbol{e}}|^{\gamma_2-1}\Big(-\boldsymbol{K}_1\boldsymbol{s}^T\boldsymbol{s} - \hat{\eta}|\boldsymbol{s}| + (\boldsymbol{\varepsilon}_m + \boldsymbol{\varepsilon}_n)\boldsymbol{s} - \widetilde{\eta}|\boldsymbol{s}|\Big) \tag{41}$$

Considering the constraint in Equation (34) yields

$$\begin{aligned}\dot{V}_2 &\le \gamma_2\boldsymbol{\beta}|\dot{\boldsymbol{e}}|^{\gamma_2-1}\boldsymbol{s}^T(-\boldsymbol{K}_1\boldsymbol{s} - \hat{\eta}\mathrm{sign}(\boldsymbol{s}) + \eta\mathrm{sign}(\boldsymbol{s}) - \widetilde{\eta}\mathrm{sign}(\boldsymbol{s})) \\ &\le -\gamma_2\boldsymbol{\beta}|\dot{\boldsymbol{e}}|^{\gamma_2-1}\boldsymbol{K}_1\boldsymbol{s}^T\boldsymbol{s} \le 0\end{aligned} \tag{42}$$

According to the Lyapunov stability criterion, it is concluded that the system's error variables will converge to zero along the sliding manifold in a finite-time. The proof is completed. □

Remark 3. *Without the disturbance observer and RBFNN approximator being introduced, substituting Equation (21) into Equation (16) leads to Equation (44); With the TANH-NTD disturbance observer and RBFNN approximator being adopted, substituting the Equation (35) into (16) leads to Equation (45). Comparing with Equations (44) and (45), it can be seen that the total dynamic uncertainties change from $\boldsymbol{D} + \boldsymbol{d}$ to $\boldsymbol{D} - \hat{\boldsymbol{D}} + \boldsymbol{d} - \hat{\boldsymbol{d}}$ by the compensatory effect of the disturbance observer and RBFNN. Therefore, the switching gain of the control law can be decreased from $\boldsymbol{K}_2$, the upper bound of the lumped uncertainties, to the estimation of the upper bound $\hat{\boldsymbol{\eta}}$, and the approximation error $\boldsymbol{D} - \hat{\boldsymbol{D}} + \boldsymbol{d} - \hat{\boldsymbol{d}}$, which can alleviate chattering.*

$$\dot{\boldsymbol{s}} = \boldsymbol{\beta}\gamma_2|\dot{\boldsymbol{e}}|^{\gamma_2-1}(\boldsymbol{D} + \boldsymbol{d} - \boldsymbol{K}_1\boldsymbol{s} - \boldsymbol{K}_2\mathrm{sign}(\boldsymbol{s})) \tag{43}$$

$$\dot{\boldsymbol{s}} = \boldsymbol{\beta}\gamma_2|\dot{\boldsymbol{e}}|^{\gamma_2-1}\big(\boldsymbol{D} - \hat{\boldsymbol{D}} + \boldsymbol{d} - \hat{\boldsymbol{d}} - \boldsymbol{K}_1\boldsymbol{s} - \hat{\boldsymbol{\eta}}\mathrm{sign}(\boldsymbol{s})\big) \tag{44}$$

Given the proceeding analysis, the detailed computational procedure of designing the NN-NFTSMC approach is described in Algorithm 1.

Algorithm 1 NN-NFTSMC

Input:
(1) The desired trajectory $\boldsymbol{x}_d$
(2) The present position and attitude $\boldsymbol{x}$
(3) Model parameters of the quadrotor
Output: Control inputs for trajectory tacking
Step 1: Design of the control input
(1) Compute the state errors: $\boldsymbol{e} = \boldsymbol{x} - \boldsymbol{x}_d$, $\dot{\boldsymbol{e}} = \dot{\boldsymbol{x}} - \dot{\boldsymbol{x}}_d$;
(2) Define the sliding surface: $\boldsymbol{s} = \boldsymbol{e} + \boldsymbol{\alpha}\text{sign}^{k_1}(\boldsymbol{e}) + \boldsymbol{\beta}\text{sign}^{k_2}(\dot{\boldsymbol{e}})$;
(3) Design adaptive laws: $\dot{\hat{\boldsymbol{W}}} = \gamma_2 \boldsymbol{\Gamma}\boldsymbol{\beta}|\dot{\boldsymbol{e}}|\boldsymbol{h}\boldsymbol{s}^T$, $\dot{\hat{\eta}} = \lambda\boldsymbol{\beta}|\boldsymbol{s}|^T|\dot{\boldsymbol{e}}|^{\gamma_2 - 1}$
(4) Construct neural network approximation and disturbance observer: $\hat{\boldsymbol{D}} = \hat{\boldsymbol{W}}^T\boldsymbol{h}$, $\hat{\boldsymbol{d}}$
(5) Calculate the control signal $\boldsymbol{u}$
Step2: Proof of the closed-loop system stabilization
(1) Select the Lyapunov candidate function V
(2) Calculate the first-order derivative of Lyapunov function $\dot{V}$
(3) Check the sign of $\dot{V}$
(4) Analyze the convergence of the state variables
Step3: Ending
If the state errors satisfy the requirement, terminate the algorithm and output the control signal u. Otherwise, go to **step1**

4. Simulation Results

In this section, numerical simulations are presented to illustrate the effectiveness of the designed control method. The physical parameters of the studied quadrotor are replicated from Ref. [24] and the reference trajectories are adopted from Ref. [30]. Subsequently, to study the performance of the designed NN-NFTSMC scheme, the global fast terminal sliding mode control (GFTSMC) method [31] and second order sliding mode control (SOSMC) method [32] will be compared by using numerical simulations. The controller parameters of NN-NFTSMC are listed in Table 1.

Table 1. Control parameters of NN-FTSMC.

Parameter	Value
$\boldsymbol{\alpha}$	diag (6, 6, 6, 0.5, 0.5, 0.5)
$\boldsymbol{\beta}$	diag (0.3, 0.3, 0.3, 0.8, 0.8, 0.8)
γ_1	1.3
γ_2	1.1
$\boldsymbol{K}_1$	diag(20, 20, 20, 10, 10, 10)
$\boldsymbol{\Gamma}$	diag(15, 15, 15, 35, 35, 35)
λ	20

4.1. Simulation 1

This simulation is conducted considering the case for $\Delta\boldsymbol{J} = 0.05\boldsymbol{J}_0$, $\Delta m = 0.05m_0$, $d_\xi = 0.1N$ and $d_\eta = 0.1N \cdot m$. To evaluate the effectiveness of the proposed controller, the GFTSMC controller is employed for comparison. The initial state of the quadrotor is $\boldsymbol{x}_0 = [0, 0, 0, 0, 0, 0]^T$, and the desired trajectory, which consists of taking-off, hovering and landing, is listed in Table 2 in terms of the reference position and yaw angle.

The trajectory tracking results of both methods are shown in Figures 4 and 5, and the tracking errors of the proposed method is displayed in Figure 6. It can be seen that both the NN-NFTSMC and GFTSMC methods are able to hold the quadrotor position and attitude steady, even though the desired position and angle are modified in every moment. However, it is obvious that the GFTSMC technique is unable to maintain the null steady error due to the coupling relationship between these state variables. The designed NN-NFTSMC controller is able to maintain the system state variables on their references without oscillation. In addition, compared with the GFTSMC technique, NN-NFTSMC

can provide more rapid response speed and take less time to drive the state errors to zero. The control inputs are displayed in Figure 7, which include the total thrust u, rotation torques τ_ϕ, τ_θ and τ_ψ. These results fully prove that the proposed NN-NFTSMC controller has advantages over the GFTSMC controller in terms of suppressing coupling, tracking accuracy and convergence rate.

Table 2. Reference position and yaw angle of the desired trajectory.

Variable	Value	Times
$[x_d(\mathrm{m}), y_d(\mathrm{m}), z_d(\mathrm{m})]$	[0.6, 0.6, 0.6]	0
	[0.3, 0.6, 0.6]	10
	[0.3, 0.3, 0.6]	20
	[0.6, 0.3, 0.6]	30
	[0.6, 0.6, 0.6]	40
	[0.6, 0.6, 0.0]	50
$\psi[(\mathrm{rad})]$	[0.5]	0
λ	[0.0]	50

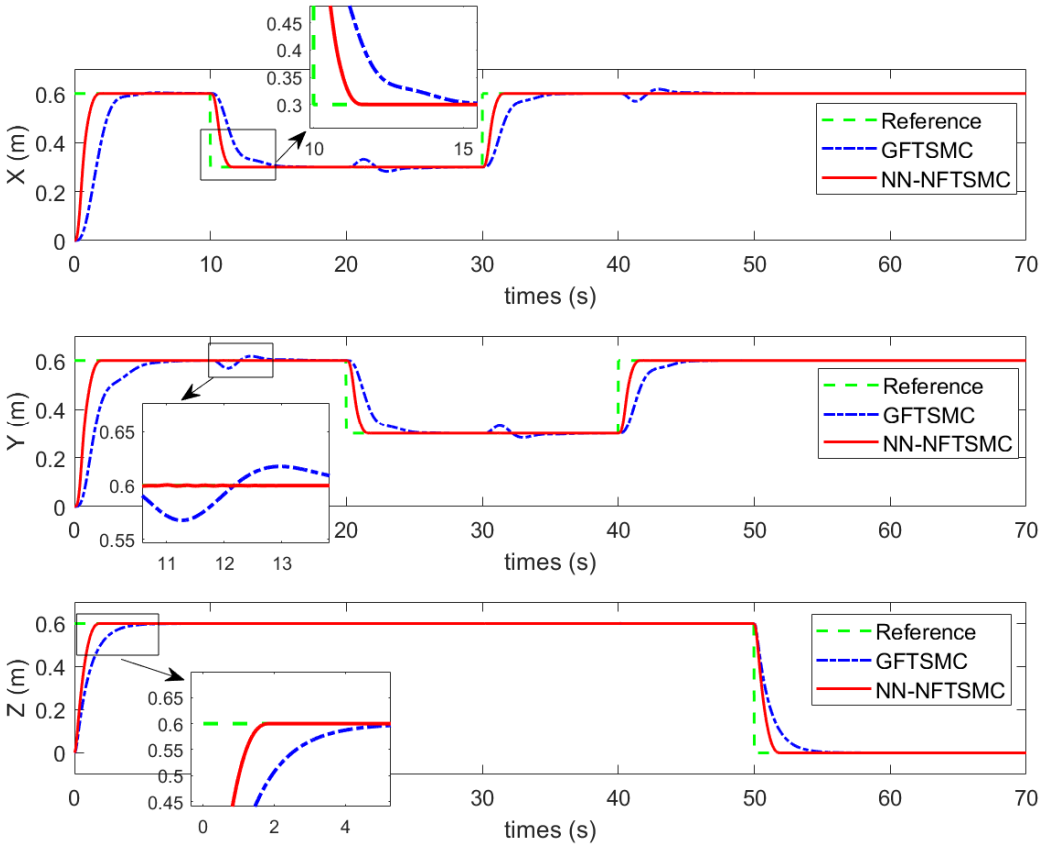

Figure 4. Position (x, y, z) in simulation 1.

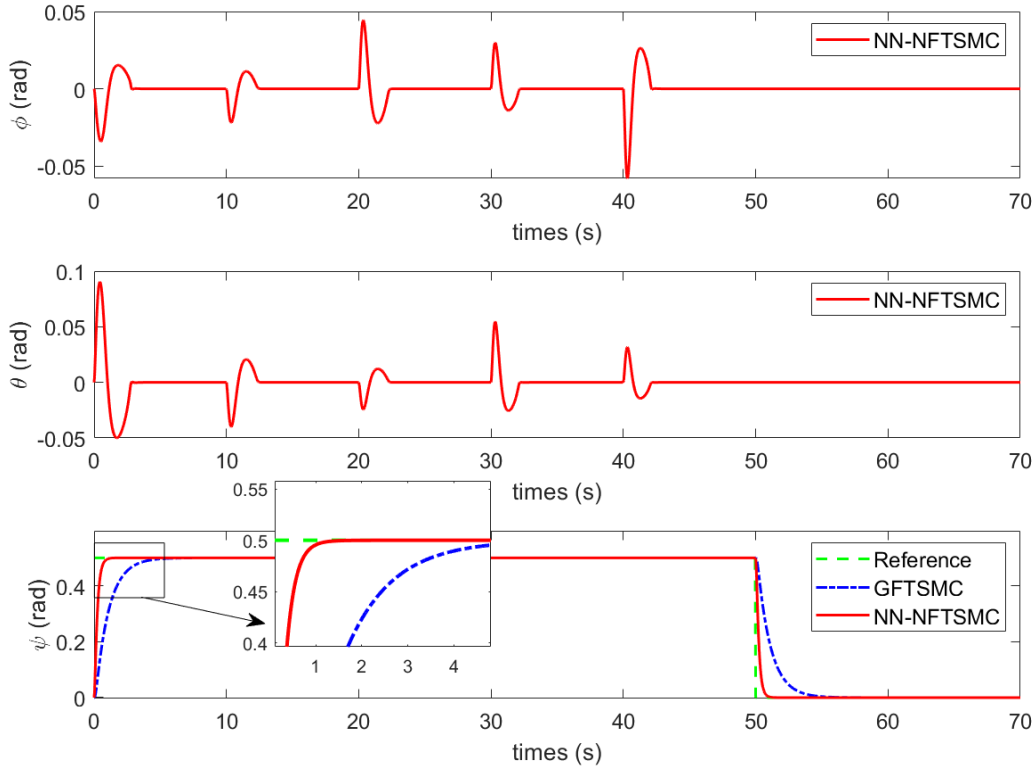

Figure 5. Attitude (ϕ, θ, ψ) in simulation 1.

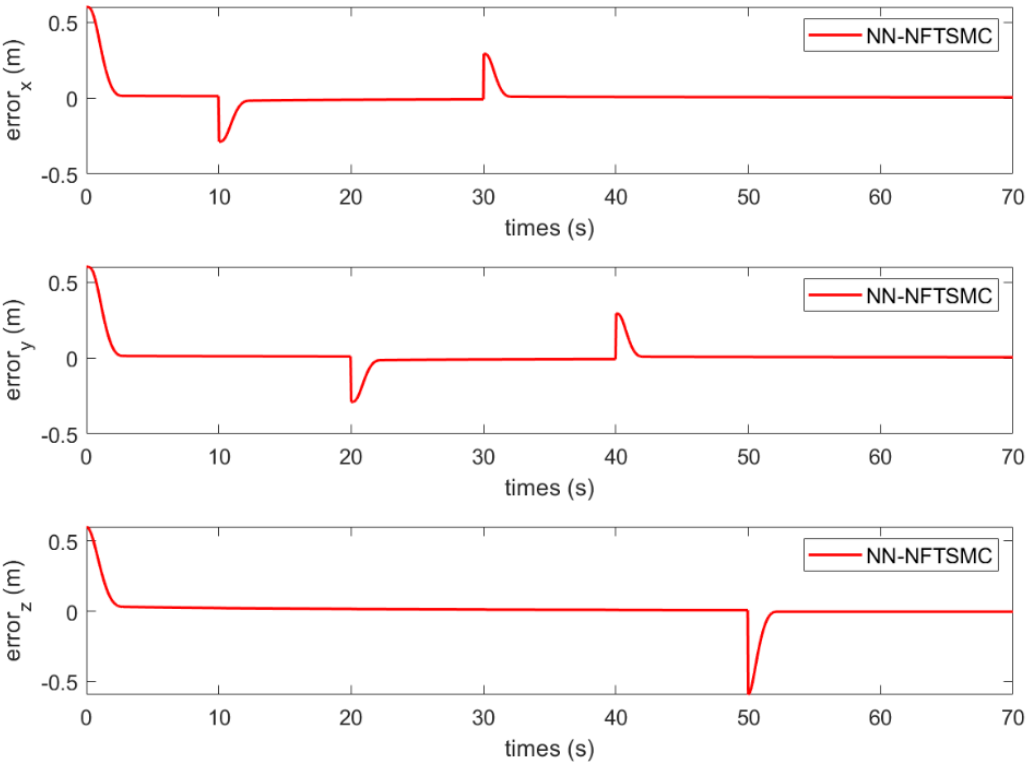

Figure 6. Position tracking errors in simulation 1.

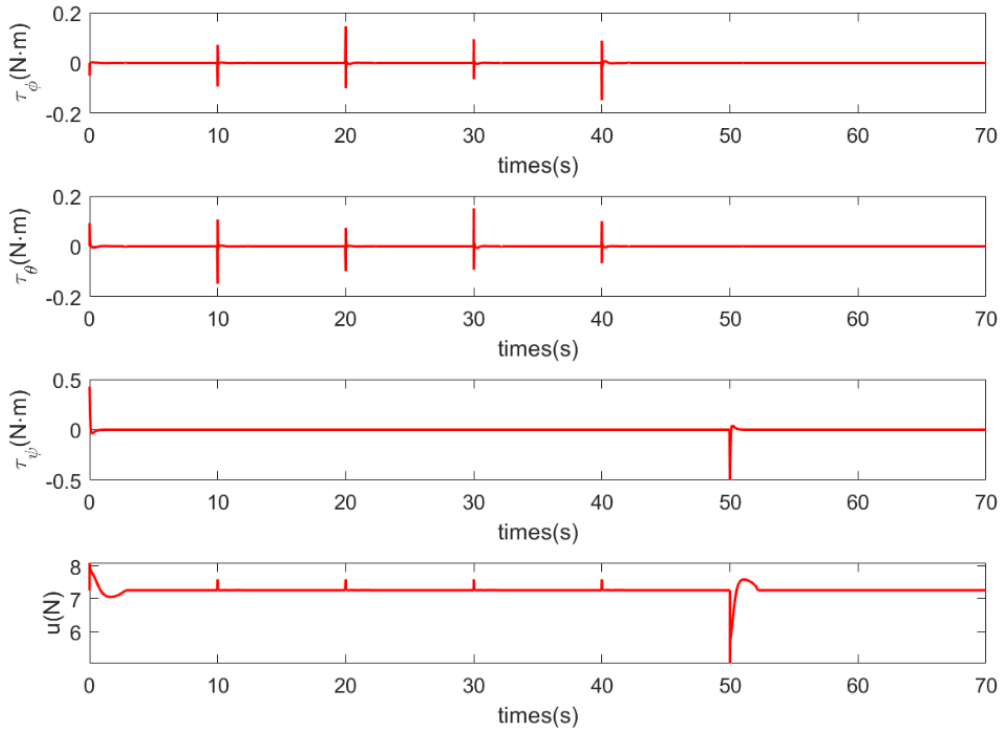

Figure 7. Control inputs in simulation 1.

4.2. Simulation 2

The tracking performance of the SOSMC method is given in the comparative simulation. The values of inertias and total mass are up to 15% overstated, i.e., $\Delta \boldsymbol{J} = -0.15\boldsymbol{J}_0$ and $\Delta m = -0.15m_0$. The external disturbance is imposed on the accelerations of position and attitude, whose expressions are given by:

$$\boldsymbol{d} = \begin{bmatrix} 0.5\sin(0.7t) \\ 0.5\sin(0.5t) \\ 0.5\cos(0.7t) \\ 0.5\sin(0.7t) \\ 0.5\sin(0.4t) \\ 0.5\sin(0.7t) \end{bmatrix} \tag{45}$$

The initial condition of the vehicle is $\boldsymbol{x}_0 = [0, 0, 0.5, 0.5, 0.5, 0.5]^T$.The desired trajectory is given as:

$$\begin{aligned} x_d &= \begin{cases} 0 & t \in [0, 55) \\ 0.3\cos\left(\frac{\pi t}{6}\right)\mathrm{m} & t \in [55, 120] \end{cases} \\ y_d &= \begin{cases} 0 & t \in [0, 55) \\ 0.3\sin\left(\frac{\pi t}{6}\right)\mathrm{m} & t \in [55, 120] \end{cases} \\ z_d &= \begin{cases} 1\mathrm{m} & t \in [0, 42) \\ 0.7\mathrm{m} & t \in [42, 87) \\ 0.8\mathrm{m} & t \in [87, 120] \end{cases} \\ \psi_d &= 0\mathrm{rad} \end{aligned} \tag{46}$$

The trajectory tracking results are depicted in Figures 8 and 9. It should be noted that, despite the presence of the dynamic uncertainties and external disturbances, the proposed controller demonstrates the better tracking performance than the SOSMC technique. It is noticeable that, starting from the initial position far from the desired trajectory, the NN-NFTSMC succeeds in maneuvering the quadrotor along the reference trajectory in a short

time and small amplitude oscillation observed. However, during flight phase involving hovering and sine-wave maneuver in the trajectory, the proposed method can maintain a satisfactory level of precision, due to the strong nonlinear fitting ability of the designed disturbance observer and RBFNN approximator. The position tracking errors are displayed in Figure 10. It can be seen that the NN-NFTSMC method is able to reject the model uncertainties and disturbances. These figures successfully illustrate that the remarkable performance of the proposed NN-NFTSMC controller.

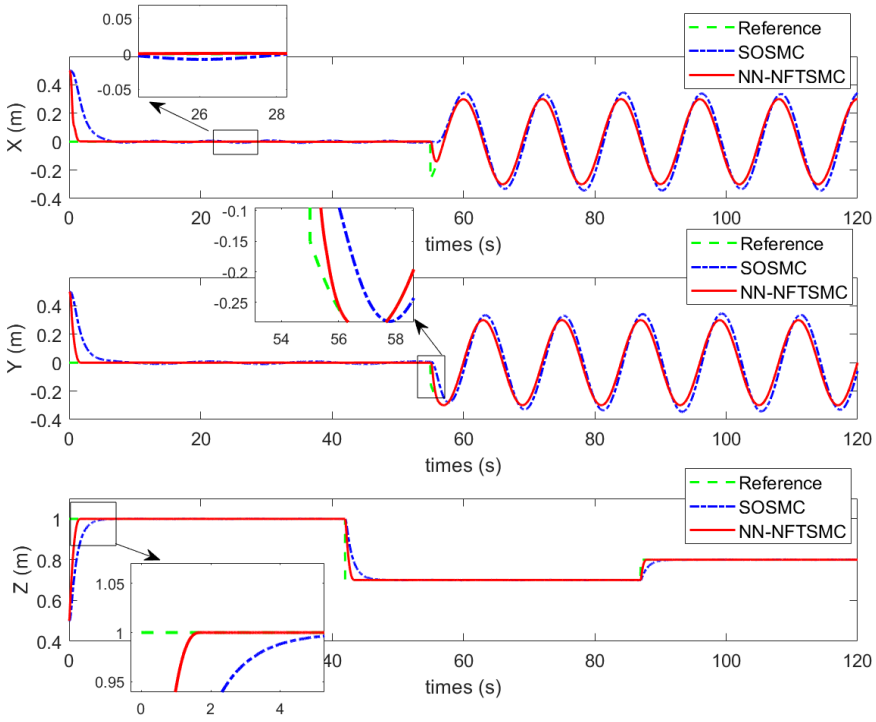

Figure 8. Position (x, y, z) in Simulation 2.

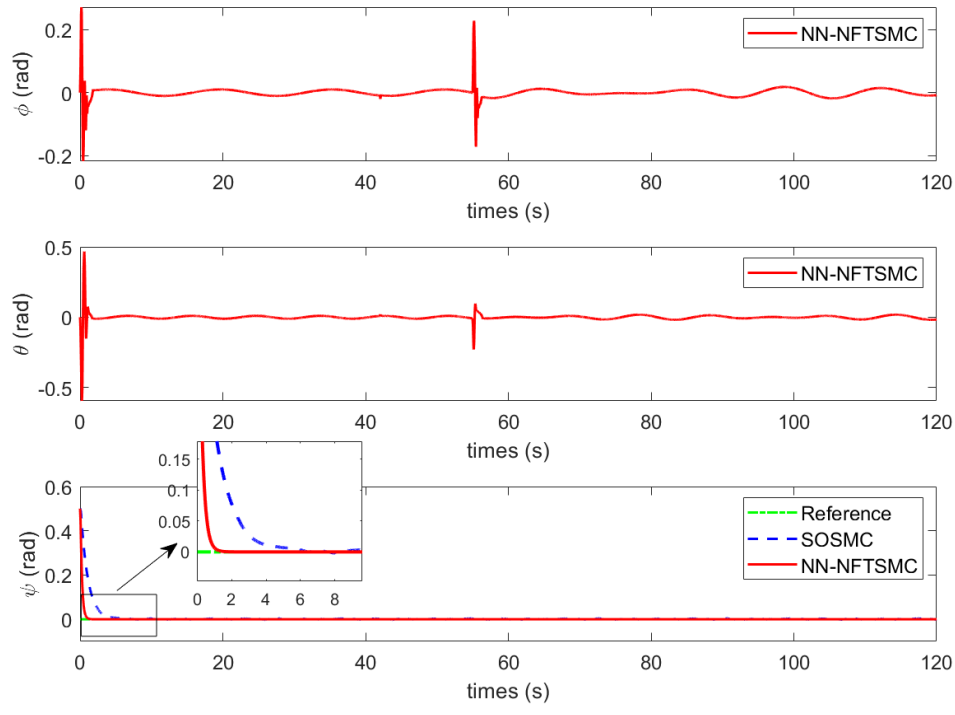

Figure 9. Attitude (ϕ, θ, ψ) in simulation 2.

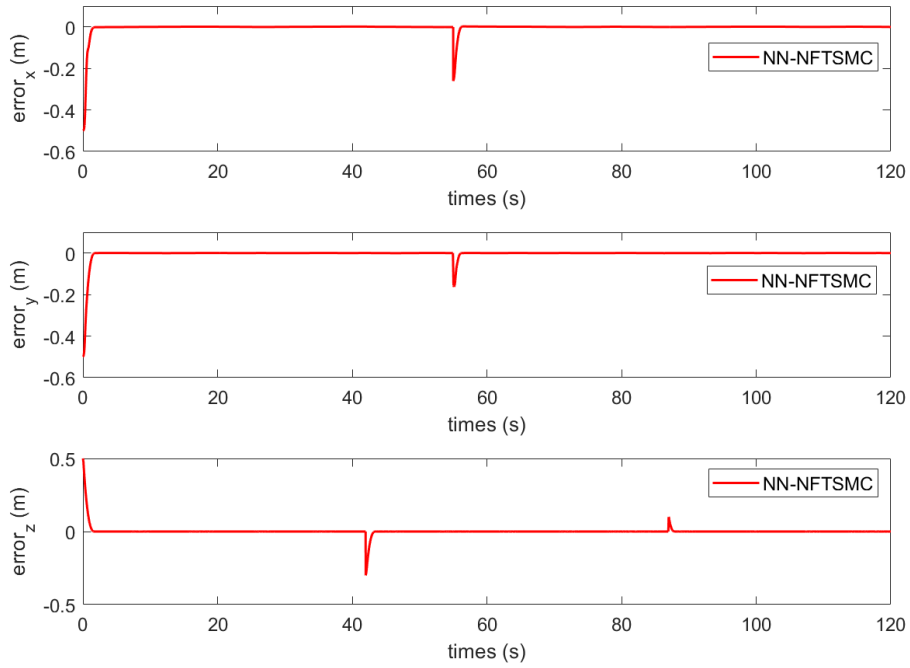

Figure 10. Position (x, y, z) tracking errors in Simulation 2.

4.3. Simulation 3

In this simulation, the values of inertias and total mass are undervalued by 15%, i.e., $\Delta \boldsymbol{J} = 0.15\boldsymbol{J}_0$ and $\Delta m = 0.15m_0$. The external disturbances are the same as those in Simulation 2. The quadrotor is initially located at $x_0 = [0, 0, 0.5, 0.5, 0.5, 0.5]^T$, and the desired trajectory is given as:

$$
\begin{aligned}
x_d &= \begin{cases} \frac{1}{2}\cos\left(\frac{t}{2}\right) \text{ m} & t \in [0, 4\pi) \\ 0.5 \text{ m} & t \in [4\pi, 20) \\ 0.25t - 4.5 \text{ m} & t \in [20, 30) \\ 3 \text{ m} & t \in [30, 80] \end{cases} \\
y_d &= \begin{cases} \frac{1}{2}\sin\left(\frac{t}{2}\right) \text{ m} & t \in [0, 4\pi) \\ 0.25t - 3.14 \text{ m} & t \in [4\pi, 20) \\ 5 - \pi \text{ m} & t \in [20, 30) \\ -0.2358t + 8.94 \text{ m} & t \in [30, 40) \\ -0.5 \text{ m} & t \in [40, 80] \end{cases} \\
z_d &= \begin{cases} 0.125t + 1 \text{ m} & t \in [0, 4\pi) \\ 0.5\pi + 1 \text{ m} & t \in [4\pi, 40) \\ \exp(-0.2t + 8.944) \text{ m} & t \in [40, 80] \end{cases} \\
\psi_d &= 0 \text{ rad}
\end{aligned}
\tag{47}
$$

The trajectory tracking performances under the model uncertainties and time-varying disturbances are presented in Figures 11 and 12. It can be seen that the proposed NN-NFTSMC method achieves the desired trajectory tracking with a faster convergence rate than that of the SOSMC method. The trajectory tracking using the NN-NFTSMC approach has much lower oscillations and overshoots. However, the SOSMC approach can hardly handle the chattering well, which is aggravated by parameter uncertainties and disturbances. Figure 13 shows the time histories of the position tracking errors with the NN-NFTSMC. The position tracking errors converge to the neighborhood of zero in finite time. During the steady state, the error accuracy of the position is on the order of 10^{-3}.Based on

above analysis, it is clear that the proposed method can provide better tracking accuracy and faster convergence rate.

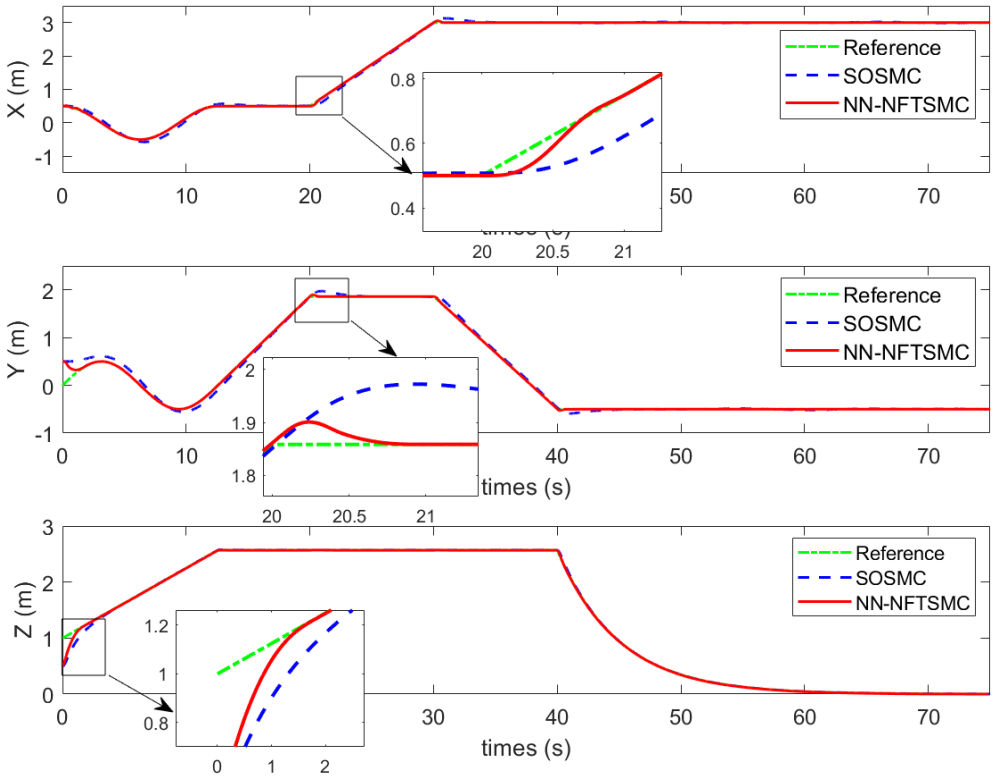

Figure 11. Position (x, y, z) in simulation 3.

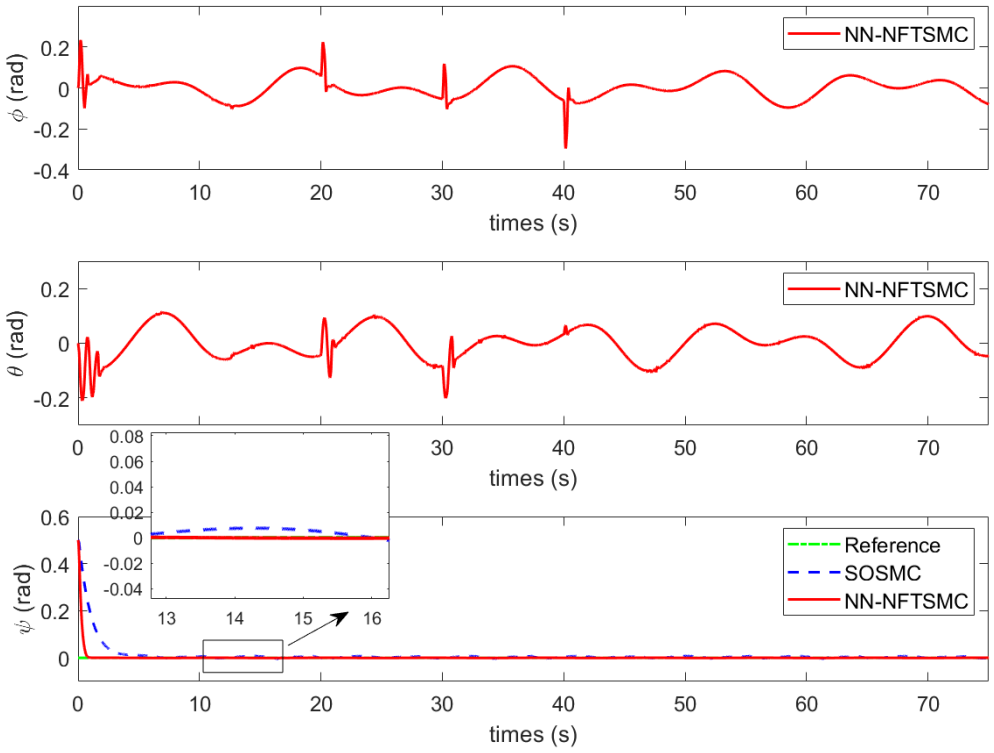

Figure 12. Attitude (ϕ, θ, ψ) in simulation 3.

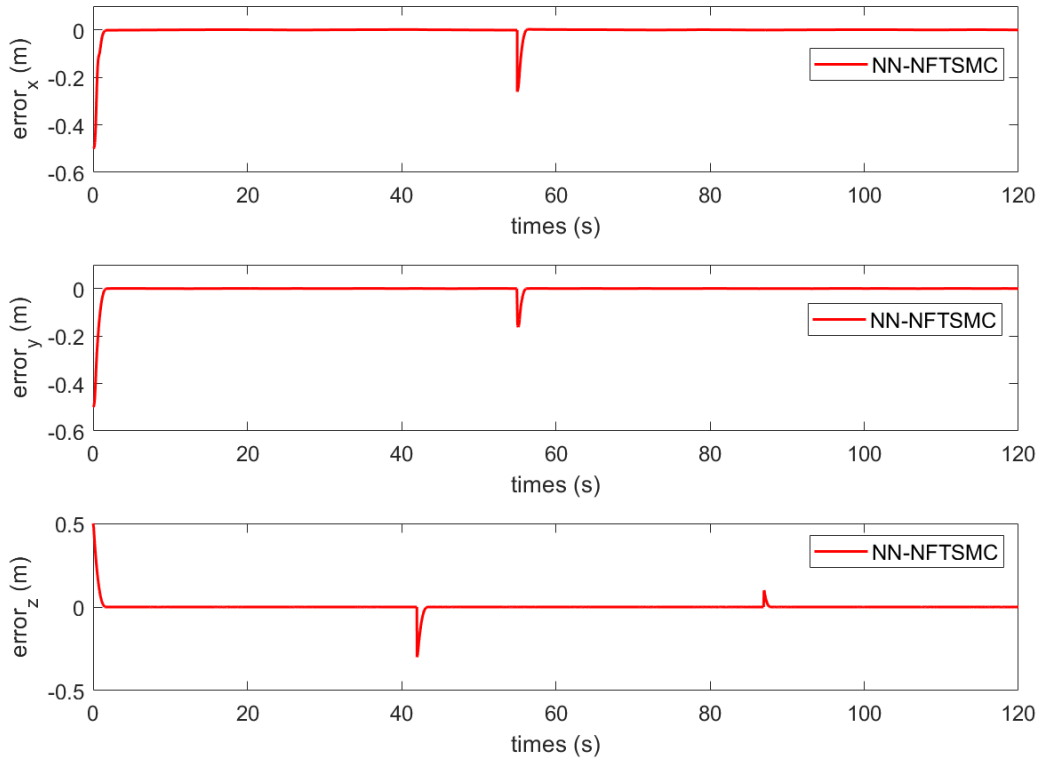

Figure 13. Position (x, y, z) tracking errors in simulation 3.

5. Conclusions

A NN-NFTSMC approach was designed to address the problem of quadrotor trajectory tracking control while being subjected to model uncertainties and disturbances. The proposed method combined the merits of NFTSMC, TANH-NTD and NN. The NFTSMC technique guaranteed the rapid finite-time convergence of all state variables with high accuracy, in which the singularity problem was avoided. Furthermore, a TANH-NTD disturbance observer and NN approximator were adopted provide an online estimate of the external disturbances and dynamic uncertainties acting on all degrees of freedom of the system. Comprehensive simulations were conducted to illustrate the enhanced performance of the proposed method.

Author Contributions: Conceptualization, S.H. and Y.Y.; methodology, S.H.; software, S.H.; validation, S.H. and Y.Y.; formal analysis, S.H.; investigation, S.H.; resources, S.H.; data curation, S.H.; writing-original draft preparation, S.H.; writing-review and editing, Y.Y.; visualization, S.H.; supervision, Y.Y.; project administration, S.H.; funding acquisition, Y.Y. All authors have read and agreed to the published version of the manuscript.

Funding: This research is funded by Chinese Postdoctoral Science Foundation (No. 47661), Fund Project of Foundation Strengthening Plan (No. 2019-JCJQ-JJ-229) and Support Program of Young Talents of Huxiang (No. 470 2019RS2029).

Institutional Review Board Statement: The study was conducted in accordance with the Declaration of Helsinki, and approved by the Institutional Review Board of National University of Defense Technology.

Informed Consent Statement: Not applicable.

Data Availability Statement: Not applicable.

Conflicts of Interest: The authors declare no conflict of interest.

References

1. Mohd, M.A. Trajectory tracking control of autonomous quadrotor helicopter using robust neural adaptive backstepping approach. *J. Aerosp. Eng.* **2018**, *31*, 04017091. [CrossRef]
2. Hu, L.; Chen, F.; Jiang, B. Control strategy for a quadrotor helicopter with state delay via improved guaranteed cost control and quantum adaptive control. *J. Aerosp. Eng.* **2017**, *30*, 04017004. [CrossRef]
3. Mo, H.; Farid, G. Nonlinear and adaptive intelligent control techniques for quadrotor UAV—A survey. *Asian J. Control* **2019**, *21*, 989–1008. [CrossRef]
4. Li, Z.; Ma, X.; Li, Y. Robust tracking control strategy for a quadrotor using RPD-SMC and RISE. *Neurocomputing* **2019**, *331*, 312–322. [CrossRef]
5. Tayebi, A.; McGilvray, S. Attitude stabilization of a VTOL quadrotor aircraft. *IEEE Trans. Control Syst. Technol.* **2006**, *14*, 562–571. [CrossRef]
6. Atheer, L.S.; Haider, A.F. Flight PID controller design for a UAV quadrotor. *Sci. Res. Essays* **2010**, *5*, 3660–3667.
7. Rinaldi, F.; Chiesa, S.; Quagliotti, F. Linear quadratic control for quadrotors UAVs dynamics and formation flight. *J. Intell. Robot. Syst.* **2013**, *70*, 203–220. [CrossRef]
8. Aboudonia, A.; El-Badawy, A. Disturbance observer-based feedback linearization control of an unmanned quadrotor helicopter. *Proc. Inst. Mech. Eng. Part I J. Syst. Control Eng.* **2016**, *230*, 877–891. [CrossRef]
9. Yang, Y.; Wu, J.; Zheng, W. Station-keeping control for a stratospheric airship platform via fuzzy adaptive backstepping approach. *Adv. Space Res.* **2013**, *51*, 1157–1167. [CrossRef]
10. Yang, Y.; Wu, J.; Zheng, W. Trajectory tracking for an autonomous airship using fuzzy adaptive sliding mode control. *J. Zhejiang Univ. Sci. C* **2012**, *13*, 534–543. [CrossRef]
11. Yang, Y.; Yan, Y. Attitude regulation for unmanned quadrotors using adaptive fuzzy gain-scheduling sliding mode control. *Aerosp. Sci. Technol.* **2016**, *54*, 208–217. [CrossRef]
12. Li, P.; Lin, Z.; Shen, H. Optimized neural network based sliding mode control for quadrotors with disturbances. *Math. Biosci. Eng.* **2021**, *18*, 1774–1793. [CrossRef]
13. Liu, E.; Yan, Y.; Yang, Y. Neural network approximation-based backstepping sliding mode control for spacecraft with input saturation and dynamics uncertainty. *Acta Astronaut.* **2022**, *191*, 1–10. [CrossRef]
14. Yang, Y.; Wu, J.; Zheng, W. Adaptive fuzzy sliding mode control for robotic airship with model uncertainty and external disturbance. *J. Syst. Eng. Electron.* **2012**, *23*, 250–255. [CrossRef]
15. Vu, Q.V.; Dinh, T.A.; Nguyen, T.V. An Adaptive Hierarchical Sliding Mode Controller for Autonomous Underwater Vehicles. *Electronics* **2021**, *10*, 2316. [CrossRef]
16. Jiang, T.; Lin, D.; Song, T. Finite-time backstepping control for quadrotors with disturbances and input constraints. *IEEE Access* **2018**, *6*, 62037–62049. [CrossRef]
17. Nekoukar, V.; Dehkordi, N.M. Robust path tracking of a quadrotor using adaptive fuzzy terminal sliding mode control. *Control Eng. Pract.* **2021**, *110*, 104763. [CrossRef]
18. Tripathi, V.K.; Kamath, A.K.; Verma, N.K. Fast Terminal Sliding Mode Super Twisting Controller for Position and Altitude Tracking of the Quadrotor. In Proceedings of the 2019 International Conference on Robotics and Automation, Montreal, QC, Canada, 20–24 May 2019.
19. Wu, G.Q.; Song, S.M. Anti-saturation attitude and orbit-coupled control for spacecraft final safe approach based on fast nonsingular terminal sliding mode. *J. Aerosp. Eng.* **2019**, *32*, 04019002. [CrossRef]
20. Nguyen, V.T.; Su, S.F.; Wang, N. Adaptive finite-time neural network control for redundant parallel manipulators. *Asian J. Control* **2020**, *22*, 2534–2542. [CrossRef]
21. Ghorbani, H.; Vatankhah, R.; Farid, M. Adaptive nonsingular fast terminal sliding mode controller design for a smart flexible satellite in general planar motion. *Aerosp. Sci. Technol.* **2021**, *119*, 107100. [CrossRef]
22. Yang, Y. Positioning control for stratospheric satellites subject to dynamics uncertainty and input constraints. *Aerosp. Sci. Technol.* **2019**, *86*, 534–541. [CrossRef]
23. Labbadi, M.; Cherkaoui, M. Robust adaptive backstepping fast terminal sliding mode controller for uncertain quadrotor UAV. *Aerosp. Sci. Technol.* **2019**, *93*, 105306. [CrossRef]
24. Eliker, K.; Grouni, S.; Tadjine, M. Quadcopter nonsingular finite-time adaptive robust saturated command-filtered control system under the presence of uncertainties and input saturation. *Nonlinear Dyn.* **2021**, *104*, 1363–1387. [CrossRef]
25. Labbadi, M.; Cherkaoui, M. Adaptive fractional-order nonsingular fast terminal sliding mode based robust tracking control of quadrotor UAV with Gaussian random disturbances and uncertainties. *IEEE Trans. Aerosp. Electron. Syst.* **2021**, *57*, 2265–2277. [CrossRef]
26. Yu, S.; Yu, X.; Shirinzadeh, B. Continuous finite-time control for robotic manipulators with terminal sliding mode. *Automatica* **2005**, *41*, 1957–1964. [CrossRef]
27. Chen, S.; Liu, W.; Huang, H. Nonsingular fast terminal sliding mode tracking control for a class of uncertain nonlinear systems. *J. Control Sci. Eng.* **2019**, *2019*, 8146901. [CrossRef]
28. Lu, L.; Wang, J. Design and application of tracking differentiator based on inverse hyperbolic tangent function. *Syst. Eng. Electron.* **2020**, *42*, 9.

29. Chen, T.; Chen, H. Approximation capability to functions of several variables, nonlinear functionals, and operators by radial basis function neural networks. *IEEE Trans. Neural Netw.* **1995**, *6*, 904–910. [CrossRef]
30. Labbadi, M.; Cherkaoui, M. Robust adaptive nonsingular fast terminal sliding-mode tracking control for an uncertain quadrotor UAV subjected to disturbances. *ISA Trans.* **2020**, *99*, 290–304. [CrossRef]
31. Xiong, J.J.; Zhang, G.B. Global fast dynamic terminal sliding mode control for a quadrotor UAV. *ISA Trans.* **2017**, *66*, 233–240. [CrossRef]
32. Zheng, E.H.; Xiong, J.J.; Luo, J.L. Second order sliding mode control for a quadrotor UAV. *ISA Trans.* **2014**, *53*, 1350–1356. [CrossRef] [PubMed]